Nuclear Physics A485 (1988) 445–460
North-Holland, Amsterdam

EMISSION OF HELIUM IONS AFTER ANTIPROTON ANNIHILATION IN NUCLEI

W. MARKIEL, H. DANIEL, T. VON EGIDY, F.J. HARTMANN, P. HOFMANN, W. KANERT and H.S. PLENDL[1]

Physik-Department, Technische Universität München, D 8046 Garching, Germany

K. ZIOCK and R. MARSHALL

University of Virginia, Charlottesville, Virginia 22901, USA

H. MACHNER and G. RIEPE

Kernforschungsanlage Jülich, D 5170 Jülich, Germany

J.J. REIDY

University of Mississipppi, University, Mississippi 38677, USA

Received 18 March 1988

Abstract: Spectra of hydrogen and helium ions emitted after stopped antiproton annihilation in nuclei have been measured with a Si-detector telescope. Targets of ^{12}C, ^{40}Ca, ^{63}Cu, ^{92}Mo, ^{98}Mo and ^{238}U were used. The ^{3}He and ^{4}He energy spectra can be fitted with the exponential function $e^{-E/T}$. The parameter T is essentially independent of the target mass number A. A simple pickup model reproduces the $^{4}He/^{3}He$ ratios as a function of Z and N (target proton and neutron number). The proton spectra from the ^{238}U target indicate that some protons are also emitted by the fission fragments.

E | ANTIPROTON-NUCLEUS ANNIHILATION ^{12}C, ^{40}Ca, ^{63}Cu, ^{92}Mo, ^{98}Mo, ^{238}U, stopped $\bar{p}$; measured ^{3}He, ^{4}He spectra; deduced spectrum shape, yields; Si particle telescope, enriched targets.

1. Introduction

The interaction of slow antiprotons with nuclei is presently the only way to investigate the interaction of antimatter with matter at low energies. Stopped antiprotons form antiprotonic atoms, emit X-rays during their cascade to low antiprotonic orbits, and annihilate with a proton or neutron. The annihilation preferentially takes place at a radius at which the nuclear density has about 10% of the central density [1]). Due to the large absorption cross section stopped antiprotons are unlikely to penetrate into the nucleus. The annihilation sets free an enormous amount of energy (1880 MeV) in the volume of only one or two nucleons [2]). It has, therefore, been

[1] Permanent address: Florida State University, Tallahassee, Florida 32306, USA.

speculated that exotic states of nuclear matter such as glueballs, quark-gluon plasma, or shock waves might be created [3-9]). In contrast to other processes involving similar amounts of energy, e.g. fast pion, proton or ion reactions, the stopped antiproton annihilation process is characterized by the low linear and angular momenta of the system, and a homogeneous angular distribution of the annihilation products. The purpose of the present investigation is to study the more ordinary processes induced by the nuclear absorption of antiprotons so that the special processes can be identified once the theory of the process has reached a level that will make specific predictions possible.

The annihilation of slow antiprotons with protons or neutrons yields in more than 95% of all events only various combinations of π^+, π^- and π^0 which are produced either directly or by decay of mesonic resonances (η, ρ, ω) [10]). The resulting pion multiplicities range from 2 to 8 with an average value of 5. The pions have energies up to nearly 1 GeV with an average of 230 MeV. During the annihilation on the nuclear surface some pions escape and some enter the nucleus and start an intranuclear cascade. Since the energy of the pions lies in the region of the Δ-resonance, they have a short range in the nucleus and transfer large amounts of energy. In direct processes pions can be absorbed or scattered, Δ-resonances or additional pions can be produced, and protons, neutrons, deuterons, tritons, He-particles or other light nuclei can be knocked out. In these processes the nucleus can be heated up to several hundred MeV [ref. [1])] and can evaporate additional particles. In a few percent of the annihilations kaons and hypernuclei are produced [11]). Recent measurements by our group of the distribution of residual nuclei after annihilation show that heavier nuclei lose between 1 and 50 nucleons [12]). Several theoretical groups have employed computer codes [1,5,13]) to calculate the intranuclear cascade, the particle emission, and the distribution of residual nuclei.

The Low Energy Antiproton Ring (LEAR) at CERN, Geneva, is an ideal facility to study antiproton-nucleus interactions. As part of a more comprehensive study of antiprotonic atoms and antiproton-nucleus annihilation, we report the measurement of the light-ion spectra with a Si-detector telescope particularly suited for ^{3}He and ^{4}He particles. ^{12}C, ^{40}Ca, ^{63}Cu, ^{92}Mo, ^{98}Mo and ^{238}U targets were used. Hydrogen-ion spectra measured with a Ge-detector telescope will be published separately.

The shapes of the spectra and the absolute and relative yields of various emitted particles are expected to shed light on the antiproton annihilation at the nuclear surface, on the consequences of the localized deposition of large amounts of energy, and on the intranuclear cascade process. This should permit one to test the assumptions underlying the various cascade calculations.

2. Experimental procedure

The experiment has been performed at an antiproton beam of LEAR. The average beam intensity was 50 000 $\bar{p}$/s, at a momentum of 202 ± 1 MeV/c. The experimental

arrangement is shown in fig. 1. The antiprotons were identified with a scintillation detector telescope consisting of an anticounter S1 (11 cm diameter, 10 mm thickness, with a 2 cm diameter hole) and a counter S2 (2 cm diameter, 1 mm thickness). Between these two detectors were two polyethylene wedges, adjusted so that the antiprotons would stop in the target. The diameter of the stopped beam was measured with a polaroid film and found to be about 18 mm. A separate measurement with copper disks as absorbers in front of an additional anticounter S3 showed that 28%, 74% and 94% of the antiprotons are stopped within circles of 8, 18 and 28 mm diameter, respectively.

In order to measure the stopping distribution in beam direction the counter S3 was mounted in the target position and run in anti-coincidence with $\overline{S1} \cdot S2$. The $\overline{S1} \cdot S2 \cdot \overline{S3}$ count rate, measured as a function of the moderator thickness, had a gaussian distribution with a FWHM of 20 mg/cm^2 of polyethylene. The stopping distribution was also determined with the $\bar{p}$ X-ray intensities from the ^{63}Cu target measured as a function of the moderator setting. For each individual target the moderator was set in such a way that the centroid of the stopping distribution was

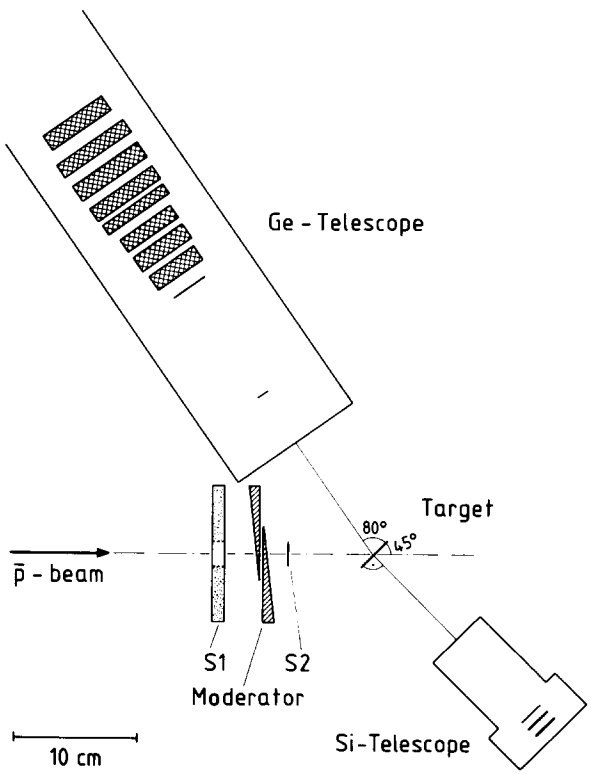

Fig. 1. Experimental arrangement at LEAR/CERN with the $\bar{p}$ telescope, the target, the Si-telescope for He ions and a Ge-telescope (to be discussed in a forthcoming publication).

approximately in the center of the target. This was checked with the $\bar{p}$ X-ray intensities from the target. With this information the fraction of the antiprotons stopped in the target was calculated. As a further check the fraction of $\bar{p}$ passing through the target was also measured directly with the $\bar{p}$ X-ray intensity of a Cu sheet placed behind each target for a short time (except in the ^{63}Cu and ^{98}Mo target cases).

The six targets used in the present experiment are listed in table 1 together with their sizes and some details necessary for the intensity calibration. The targets were selected to cover a broad range of atomic masses and to study possible isotope effects in Mo. The intensity calibration factor F (counts/$\bar{p}$ per 10^6 measured counts) was calculated from the total $\bar{p}$ telescope counts $N_{\bar{p}}$, the calculated percentage α of $\bar{p}$ stopped in the target and the efficiency ($\varepsilon \approx 1$) and the solid angle ω of the particle telescope:

$$F = 1/(N_{\bar{p}} \cdot \alpha \cdot \omega)$$

with ω = detector area/4π(distance target-detector)^2.

The particle telescope consisted of three Si surface barrier detectors mounted at distances of 7 mm from each other in an aluminium holder that was flushed continuously with dry nitrogen. The three detectors had active areas of 400 mm^2

TABLE 1

Targets used in the experiment

Isotope	^{12}C	^{40}Ca	^{63}Cu	^{92}Mo	^{98}Mo	^{238}U
enrichment (%)	98.9	96.9	~98%	98.3	97.2	≥99.3
area (mm × mm)	50 × 50	22 × 30	21 × 29	25 × 30	25 × 30	20 × 40
thickness (mg/cm^2) (effective thickness $\sqrt{2}$ larger)	23	50	41	100	100	30
FWHM of stopping distribution in the target (mg/cm^2)	25 (4)	31 (5)	41 (7)	45 (8)	46 (7)	82 (26)
calculated percentage α of stopped $\bar{p}$	74 (5)	75 (3)	66 (5)	79 (2)	77 (2)	35 (11)
measured percentage of stopped $\bar{p}$	74 (5)	75 (4)	[a])	72 (12)	[a])	31 (6)
number of $\bar{p}$ telescope ($\overline{S1} \cdot S2$) events (in $10^6\bar{p}$)	383.3	295.8	259.6	154.3	179.5	265.0
distance target-particle telescope (mm) (to detector 2)	270 (3)	270 (3)	270 (3)	205 (3)	205 (3)	205 (3)
intensity calibration factor F (counts/$\bar{p}$ per 10^6 measured counts)	8.1 (6)	10.3 (6)	13.4 (11)	10.8 (5)	9.6 (5)	14.2 (45)

[a]) The measurement with a Cu sheet placed behind the target was not made for ^{63}Cu and ^{98}Mo.

and thicknesses of 0.2, 1.0 and 1.0 mm corresponding to 47, 233 and 233 mg/cm^2, respectively. In order to be able to identify a particle by the telescope the particle had to stop in either the second or the third detector, i.e. it had to have an energy $E_1^{max}(m, z) < E \leq E_3^{max}(m, z)$, where $E_i^{max}(m, z)$ is the maximum energy a particle of mass m and charge z can have and still stop in detector i. Table 2 lists the values $E_i^{max}(m, z)$ which were calculated from proton ranges [14]) in Si scaled with the Bethe formula for the other particles. Detectors 2 and 3 were calibrated with the Compton edge of the 662 keV γ-line of ^{137}Cs decay, detector 1 with the maximum energy deposited by protons (4.8 MeV). The entire telescope was tested with 54 MeV α-particles from the cyclotron at the Institut für Strahlen- und Kernphysik of the University of Bonn; the fraction of α-particles not registered with the proper energy signal (e.g. due to reactions) was 2.4%. The percentage of α-particles scattered out was estimated according to ref. [15]) to be about 0.2%.

TABLE 2

Maximum energies E_1^{max}, E_2^{max} and E_3^{max} of particles stopped in detectors 1, 2 and 3, respectively; these energies correspond to the range in 47, 280 and 513 mg/cm^2 Si, respectively (energies in MeV)

Particle	E_1^{max}	E_2^{max}	E_3^{max}
p	4.8	12.2	19.1
d	6.3	16.3	25.7
t	7.4	19.4	30.6
^{3}He	17.1	43.0	67.4
^{4}He	19.2	48.6	76.2
^{6}He	22.5	64.3	90.8
^{5}Li	33.9	94.4	132.8
^{6}Li	36.5	102.1	143.8
^{7}Li	38.9	109.7	153.8

Particle telescope signals in coincidence with the $\bar{p}$ telescope were analyzed by ADC's (Ortec AD811). The data was collected with a PDP 11/34 in list mode. The average count rate was 100/s and the dead time losses of the whole system were <5%.

The Ge telescope in fig. 1 was used for simultaneous detection of H ions.

3. Evaluation

Table 2 shows that the energy window of the telescope is rather narrow in the case of hydrogen ions. We have, therefore, concentrated in this paper on ^{3}He and ^{4}He spectra. More complete hydrogen energy spectra were measured with the Ge detector system. The particles were identified with the standard ΔE-E method. The ΔE-E plots of the ^{12}C and ^{238}U targets (fig. 2) illustrate the quality of our data.

The parameter B identifies the particle:

$$B = ((E_1 + E_2)^b - E_2^b)/d_1$$

if the particle stops in detector 2, and

$$B = ((E_1 + E_2 + E_3)^b - E_3^b)/(d_1 + d_2)$$

if the particle stops in detector 3.

E_i and d_i are the energy deposition in and thickness of detector i, respectively; the exponent b was determined from our data to have the value $b = 1.72$ for hydrogen ions and $b = 1.76$ for helium ions. Appropriate ranges for B were obtained experimentally so that most events could be identified. Fig. 2 shows that the background was negligible and that most events did have an unambiguous signature. ^{6}He and even some ^{8}He and Li ions are visible. Some Li events fall on a horizontal line in fig. 2 due to saturation in the amplifier of detector 1.

The measured energy of a particle $E = E_1 + E_2 + E_3$ does not equal the primary energy E_p with which that particle was produced, because some energy is lost in the target and in the material between the target and the first Si detector. Since it is not known where in the target an individual particle was produced, it is not possible to correct for these losses ΔE event by event. It is, however, possible to apply a global correction to the measured spectra and to derive the primary energy spectra. For each individual particle with a measured energy E an approximate

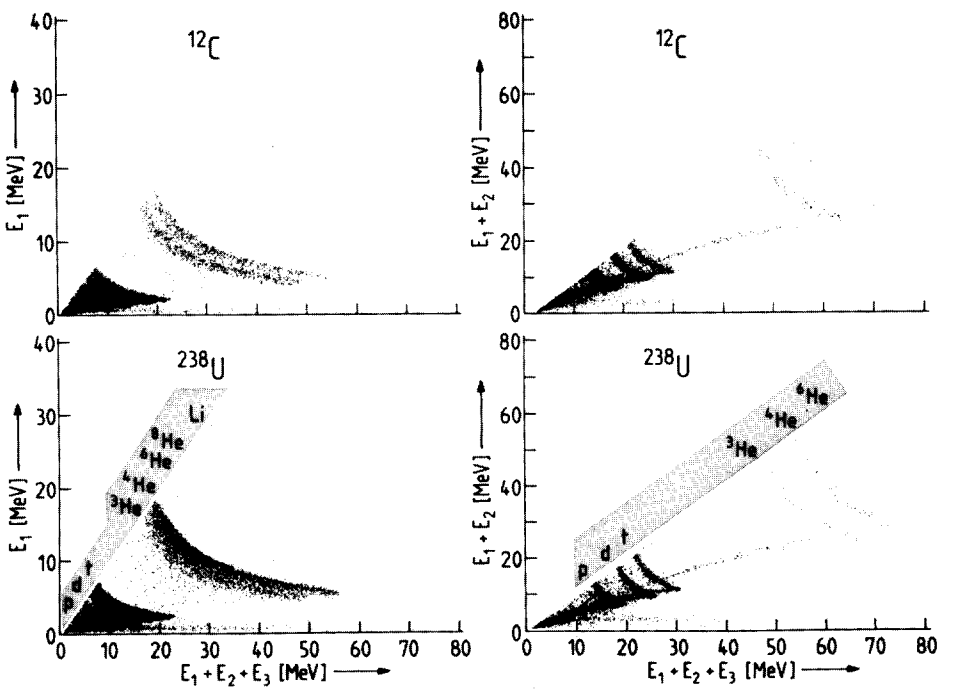

Fig. 2. ΔE-E-plot of the measured ^{12}C and ^{238}U spectra. The left side shows particles stopped in detector 2 ($E_3 = 0$).

probability distribution of the origin in the target can be determined. This probability distribution is given by the $\bar{p}$ stopping distribution in the target weighted with the spectral shape (essentially an exponential function $w(E) = e^{E/T}$ as shown later). This weight is necessary because particles that start out with a primary energy $E_p = E + \Delta E$ and traverse the target are less frequent than particles that start out with an energy $E_p = E$ and do not traverse the target, due to the decreasing energy spectrum.

For the computer calculation of this global correction the target was divided into 30 layers k with the stopping distribution g_k and $\sum g_k = 1$. The weighted stopping distribution is $g'_k = w(E_k)g_k / \sum_{k'}, (w(E_{k'})g_{k'})$ with $E_k = E + \Delta E_k$, where ΔE_k is the energy loss of a particle with measured energy E coming from layer k; ΔE_k is calculated from energy loss tables [14]).

The measured spectrum is divided into 1 MeV energy bins n with mean energy E_n and intensity $I(E_n)$. The primary spectrum is also divided in 1 MeV bins p with E_p and $I(E_p)$. The correction procedure transfers the measured intensities $I(E_n)$ of bin n via the target layers k into the primary intensity $I(E_p)$ of the energy bin p:

$$I(E_p) = \sum_n \sum_k g'_k I(E_n) \delta(p, n, k) ,$$

where $\delta(p, n, k) = 1$ if E_p is the energy bin lying next to $(E_n + \Delta E_{k,n})$ and $\delta(p, n, k) = 0$ otherwise. Energy straggling was neglected.

The spectral shape $w(E)$ is determined in an iterative procedure; it causes, however, only a small correction. The value of g_k is given by assuming a gaussian stopping distribution with the widths of table 1. Fig. 3 shows the ^{4}He spectrum of ^{63}Cu before and after correction; a significant shift to higher energies is observed.

The corrected ^{3}He and ^{4}He spectra are displayed in figs. 4 and 5, respectively. The spectra were fitted in the energy range from 35 MeV to 70 MeV with the simple

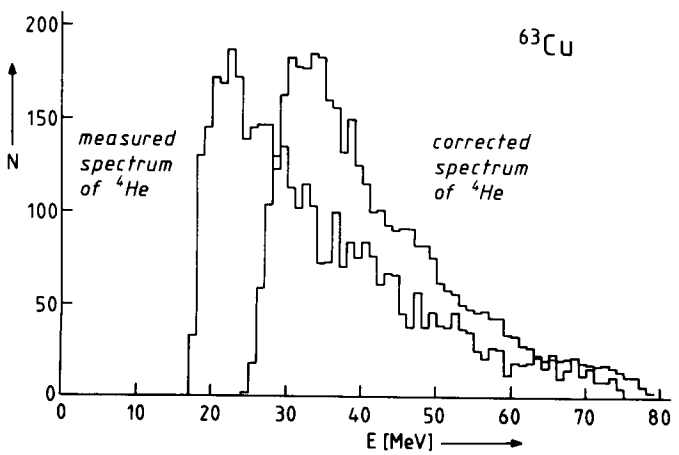

Fig. 3. Measured and corrected ^{4}He spectrum of the ^{63}Cu target.

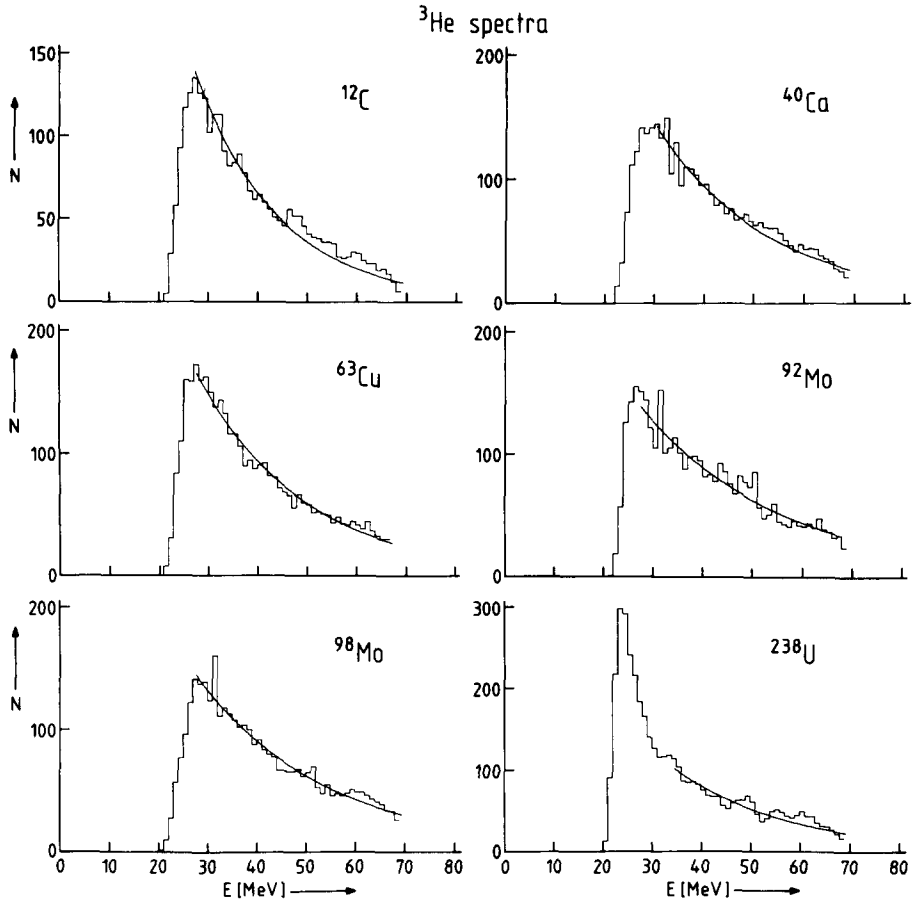

Fig. 4. Corrected ^{3}He spectra with exponential fits.

exponential function

$$N(E) = C\, e^{-E/T}.$$

The low energy cut-off of the spectra is caused by the thickness of the target and detector 1. The fitted exponential functions show in most cases good agreement with the experimental spectra. The fitted parameters T and the averages T_0 over the six targets are given in table 3.

^{3}He and ^{4}He yields (per 100 stopped antiprotons) in given energy windows and the ^{4}He/^{3}He ratios in different energy or momentum windows are listed in table 4. Since the energy window of the telescope for hydrogen ions was very small and since the yields of the ^{6}He, ^{8}He and Li components were very low, an exponential function could not be fitted in these cases and only total measured yields are given in table 5. Consequently, only a qualitative interpretation of this data is meaningful.

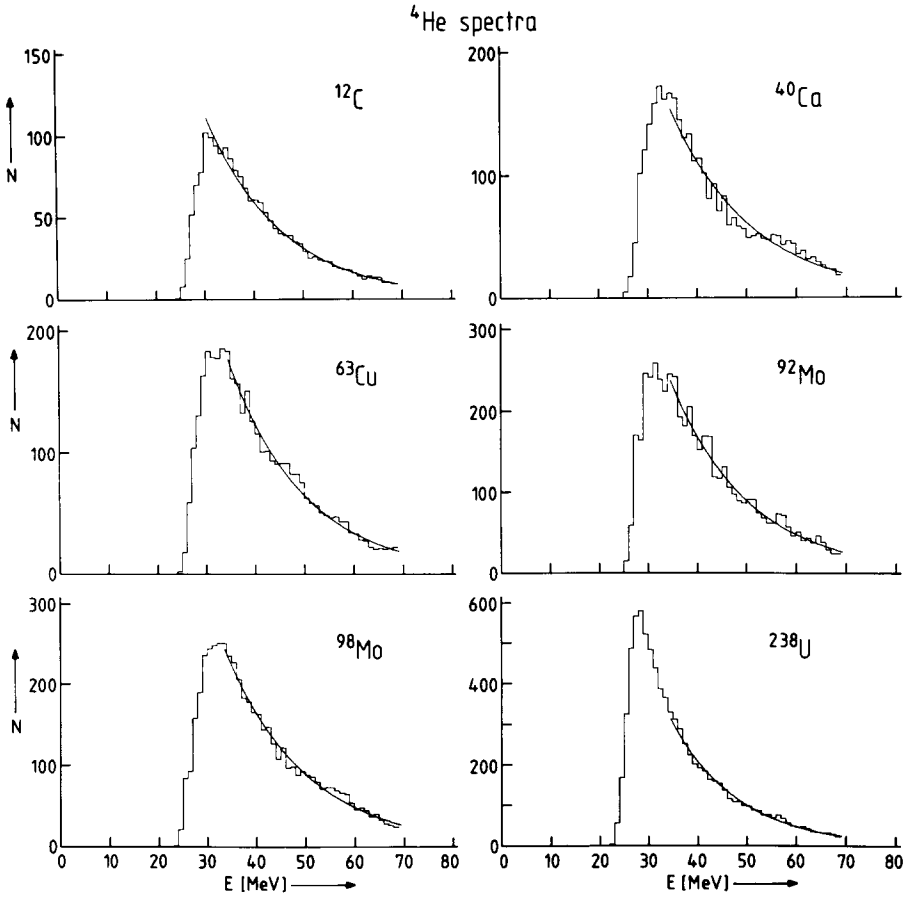

Fig. 5. Corrected ^{4}He spectra with exponential fits.

TABLE 3

Fitted values of the parameter T of the ^{3}He and ^{4}He spectra (in MeV)

	^{12}C	^{40}Ca	^{63}Cu	^{92}Mo	^{98}Mo	^{238}U	Average
^{3}He	19.8 (12)	24.2 (13)	22.2 (10)	25.2 (17)	21.8 (6)	20.1 (12)	21.9
^{4}He	15.6 (9)	16.8 (9)	15.4 (8)	16.2 (9)	17.1 (7)	14.2 (4)	15.3

TABLE 4

Yields per 100 $\bar{p}$ and yield ratios of the ^{3}He and ^{4}He spectra

	^{12}C	^{40}Ca	^{63}Cu	^{92}Mo	^{98}Mo	^{238}U
yield of ^{3}He per 100 $\bar{p}$						
36–70 MeV	1.72 (4) (13)	2.22 (5) (12)	2.60 (6) (21)	2.33 (5) (11)	2.06 (4) (10)	2.66 (6) (84)
yield of ^{4}He per 100 $\bar{p}$						
36–70 MeV	1.14 (3) (9)	2.18 (5) (11)	3.25 (7) (26)	3.78 (6) (17)	3.69 (6) (17)	5.94 (9) (190)
^{4}He/^{3}He ratio						
36–70 MeV	0.66 (2)	0.98 (3)	1.25 (4)	1.63 (4)	1.80 (9)	2.24 (10)
^{4}He/^{3}He ratio						
36–40 MeV	0.78 (5)	1.39 (7)	1.55 (8)	2.12 (10)	2.26 (23)	3.06 (22)
40–50 MeV	0.74 (5)	1.12 (5)	1.29 (6)	1.73 (7)	1.82 (16)	2.35 (17)
50–60 MeV	0.53 (5)	0.86 (5)	1.07 (7)	1.34 (7)	1.60 (18)	1.75 (16)
60–70 MeV	0.50 (6)	0.80 (6)	0.87 (6)	1.09 (8)	1.36 (19)	1.39 (17)
^{4}He/^{3}He ratio						
512–572 MeV/c	1.00 (6)	1.69 (7)	2.01 (9)	2.39 (9)	2.55 (21)	3.37 (32)
572–631 MeV/c	1.14 (9)	1.40 (9)	1.69 (10)	2.17 (12)	2.47 (28)	3.19 (32)

The first error is the statistical error, the second is the systematic error from range curve (position and width) and solid angle.

TABLE 5

Total measured yields of p, d, t, ^{6}He, ^{8}He and Li per 100 $\bar{p}$

Particle	Approximate energy range (MeV)	^{12}C	^{40}Ca	^{63}Cu	^{92}Mo	^{98}Mo	^{238}U
p	6–18	23.3 (2) (18)	74.2 (3) (38)	94.5 (4) (78)	127.2 (4) (58)	124.3 (3) (64)	76.6 (3) (240)
d	8–24	9.3 (1) (7)	18.1 (2) (9)	28.0 (2) (23)	29.0 (2) (13)	30.4 (2) (15)	31.3 (2) (99)
t	11–29	4.5 (1) (3)	5.7 (1) (3)	9.9 (1) (8)	11.8 (1) (5)	12.7 (1) (7)	18.8 (2) (59)
^{6}He	39–89	0.025 (5) (2)	0.045 (7) (3)	0.048 (8) (4)	0.061 (8) (3)	0.060 (8) (3)	0.150 (20) (50)
^{8}He	44–90	0.0041 (18) (3)	0.014 (4) (1)	0.0094 (36) (8)	0.011 (3) (1)	0.013 (4) (1)	0.041 (8) (13)
Li	61–96	0.017 (4) (2)	0.075 (9) (4)	0.058 (9) (5)	0.086 (9) (4)	0.083 (9) (4)	0.180 (16) (60)

The first error is statistical, the second one systematic.

4. Discussion of the spectrum shapes

The parameter T (table 3) does not represent a nuclear temperature, since most of the particles are apparently emitted before the nucleus has reached thermal equilibrium. However, T is related to the average energy of the emitted particles. Table 3 shows that T is essentially independent of the target mass number A with average values of $T_0 = 21.9$ MeV for ^{3}He and $T_0 = 15.3$ MeV for ^{4}He. The conversion of the average values from energy to momentum gives $p_0 = 351$ MeV/c for ^{3}He and $p_0 = 338$ MeV/c for ^{4}He. It is thus possible to describe the ^{3}He and ^{4}He spectra with the same approximate equation

$$N(E) = N_0 \, e^{-p^2/p_0^2} \qquad \text{where } p_0 = 345 \text{ MeV}/c .$$

N_0 is of course different for ^{3}He and ^{4}He. The value of p_0 is very similar to the known average momentum $p_\pi = 350$ MeV/c of pions emitted in the annihilation of $\bar{p}$ with isolated protons [1]).

Experiments with energetic protons and pions on a variety of nuclei have shown similar results. The spectra of p, d, t, ^{3}He and ^{4}He particles resulting from the bombardment of Mg, Ni and Ag with 235 MeV pions showed [16]) that the shapes are independent of the target mass and gave values of T of ~20 MeV for ^{3}He and ~17 MeV for ^{4}He. The proton spectra from the bombardment of C, Al, Ti, Cu, Cd and Pb targets with negative pions of 1.5-6.2 GeV/c and protons of 9 GeV/c [ref. [17])] were fitted with the function e^{-Bp^2} where B was found to be independent of the target nucleus A and of the nature and energy of the bombarding particles. A recent study [18]) of ^{3}He and ^{4}He spectra from 70 and 160 MeV π^+ on Ag gave values of T of 25 and 13 MeV for ^{3}He and ^{4}He, respectively.

This similarity of particle spectra emitted after $\bar{p}$ annihilation in nuclei and after bombardment with energetic pions and protons point to general and simple laws for the interaction of fast particles with nuclear matter.

The ^{3}He and ^{4}He spectra from the ^{238}U target (figs. 4 and 5) indicate that there is a significant enhancement near 25 and 30 MeV, respectively. This is probably due to stronger evaporation of helium ions in very heavy nuclei.

5. Interpretation of yields and the pickup model

The ^{3}He yields increase by a factor of about 1.5 from C to U and the ^{4}He yields by about a factor of 5. This difference is reflected by the increasing ^{4}He/^{3}He ratio with A. The ^{3}He and ^{4}He yields are larger for ^{238}U than for the other targets. Recent experiments at LEAR which investigated $\bar{p}$-^{238}U reactions [19-21]) showed that in nearly all cases fission takes place. The large ^{3}He and ^{4}He yields indicate that the fission process does not too much reduce or influence the particle emission process. The smaller proton yield of the ^{238}U target between 6 and 18 MeV is caused by the Coulomb barrier near 15 MeV. The calculation of the intranuclear cascade [22])

including particle emission has to verify these assumptions which would mean that the fission process provides a time scale.

In order to understand the yield ratios, especially the $^4He/^3He$ ratio, as functions of Z and N, a simple pickup model is proposed which uses for the calculation of the $^4He/^3He$ ratio only Z and N and one free pickup parameter. The model which was briefly described in ref. [23]) assumes that the formation of heavier emitted particles is a consecutive process and that lighter ions either escape from the nucleus or pick up protons or neutrons to become heavier ions. The pick up probabilities are assumed to be proportional to Z or N, to the dimension of the nucleus ($\propto A^{1/3}$) and to the pickup parameters r_i. This consecutive pickup scheme is shown in fig. 6 together with the corresponding pickup probabilities. It is assumed that proton and neutron pickup rates are similar. The effective pickup rates are always the result of a competition between pickup and stripping. The differential proton or neutron pickup probabilities are $(Z/A)r_i\,dR$ or $(N/A)r_i\,dR$, respectively, where dR represents a distance of travel in the nucleus. These probabilities have to be integrated over the size of the nucleus. The average integration length is proportional to $A^{1/3}$ and the proportionality factor can be included in r_i. Since a deuteron can pick up a proton or neutron, the total pickup probability is $\{(Z/A)r_2+(N/A)r_2\}\,dR = r_2\,dR$ and the factors Z/A and N/A have to be added after the integration, while ^3He and t have only one pickup channel each.

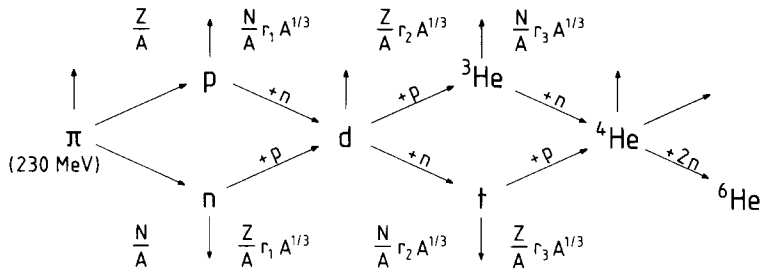

Fig. 6. Pickup model for the formation of heavier particles. The arrows mean either escape (vertical arrows) or strikes by a pion or pickup of a proton or neutron. Differential pickup probabilities are also given.

The $^4He/^3He$ ratio is calculated with the following probabilities: ^3He formation without additional n pickup: $(Z/A)\,(1-e^{-r_2A^{1/3}})e^{-(N/A)r_3A^{1/3}}$; ^4He formation via ^3He: $(Z/A)(1-e^{-r_2A^{1/3}})(1-e^{-(N/A)r_3A^{1/3}})$; ^4He formation via t: $(N/A)(1-e^{-r_2A^{1/3}})\times(1-e^{-(Z/A)r_3A^{1/3}})$; this yields:

$$R(^4He/^3He)=\frac{(1-e^{-(N/A)r_3A^{1/3}})+(N/Z)(1-e^{-(Z/A)r_3A^{1/3}})}{e^{-(N/A)r_3A^{1/3}}}.$$

The $^4He/^3He$ ratio for the energy interval from 35 to 70 MeV as a function of A is displayed in fig. 7. The pickup parameter was fitted to be $r_3 = 0.24$. The agreement

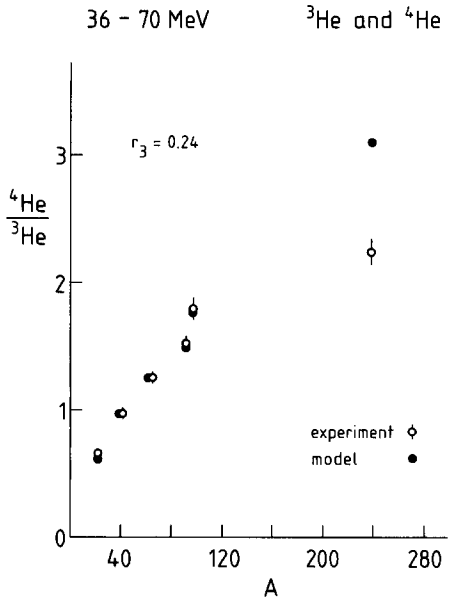

Fig. 7. Experimental and calculated $^4He/^3He$ ratios for energies from 35 to 70 MeV as a function of A.

between experiment and model is very good except for ^{238}U where the calculated value is too large. The reason for this discrepancy might be that the Coulomb barrier was not taken into account which results in tritons prefering to escape rather than to pick up a proton. Calculating the pickup parameters with the $^4He/^3He$ ratios for the energy bins 35-40, 41-50, 51-60 and 61-70 MeV, one finds the values for r_3 to be to 0.28, 0.24, 0.20 and 0.18, respectively. This behaviour indicates that the pickup probability decreases with the energy. The pickup parameter r_3 was also calculated with $^4He/^3He$ ratios for the momentum bins 512-572 and 572-631 MeV/c, resulting in $r_3 = 0.31$ and $r_3 = 0.30$, respectively. It is expected that the $^4He/^3He$ ratio is independent of the momentum, since the ^3He and ^4He spectra have the same shape proportional to e^{-p^2/p_0^2}.

The ^6He, ^8He and Li yields (table 5) show more or less pronounced increase with A. Of course, these yields are very low in the case of the ^{12}C target.

6. Evidence for proton emission by fission fragments of U

The corrected proton spectra between 6 and 18 MeV from the ^{98}Mo and ^{238}U targets are shown in fig. 8. The spectrum from ^{98}Mo indicates that the sensitivity of the telescope is zero below 5 MeV and reaches its full value at 8 MeV. The corresponding spectrum from the ^{238}U target looks quite different. The spectrum increases slowly between 5 and 15 MeV where it reaches its maximum intensity. The Coulomb barriers of ^{238}U and ^{226}Ra (i.e. after some particle emission) are 15.3 and 14.9 MeV,

respectively, as indicated in fig. 8. The energy loss in the target causes an energy resolution of a few MeV, but no protons are expected to be detected below 10 MeV. The protons observed between 5 and 10 MeV give, therefore, some evidence that protons are also evaporated from fission fragments which have Coulomb barriers between 9 and 10 MeV. Calculations [1]) indicate that residual nuclei after prompt particle emission can have excitation energies of several hundred MeV. When these hot nuclei undergo fission, the hot fission fragments can evaporate neutrons as well as protons. Since about 40% of the protons in the spectrum of ^{238}U in fig. 8 have an energy <12 MeV and the total number of protons is 77 (24) per 100 $\bar{p}$ (table 5), we find that on the average at least 17 (5)% of the fission fragments evaporate a proton. Another explanation of the low-energy protons could be the emission during the fission process.

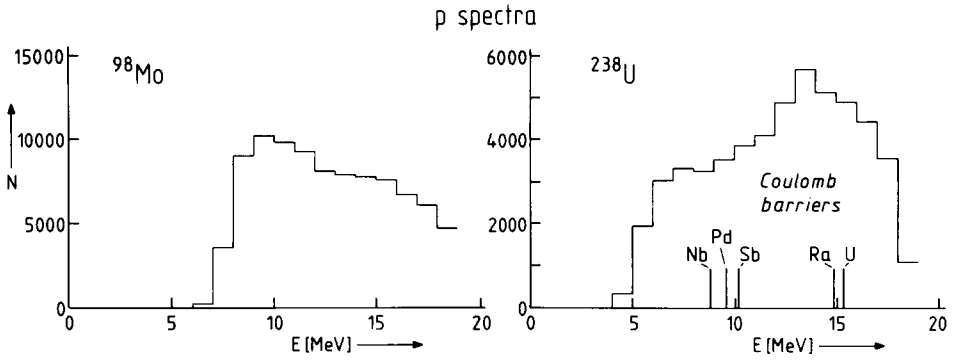

Fig. 8. Corrected p spectra from ^{98}Mo and ^{238}U targets measured with the Si telescope which identifies protons between 5 and 19 MeV. The protons of the ^{238}U target below about 10 MeV are probably emitted by fission fragments.

7. Conclusion

The measurement of charged particles emitted following the annihilation of stopped antiprotons in ^{12}C, ^{40}Ca, ^{63}Cu, ^{92}Mo, ^{98}Mo and ^{238}U targets has given detailed information on the shape and the yield of the ^{3}He and ^{4}He spectra. The shape of the spectra is independent of A, in agreement with similar results from fast proton and pion reactions. The ^{3}He and ^{4}He spectra can be reproduced with the same $p_0 = 345$ MeV/c in the formula $N(E) = N_0 \, e^{-p^2/p_0^2}$. The dependence of the ^{4}He/^{3}He ratio on Z and N was calculated with a simple pickup model; good agreement was obtained (with the exception of ^{238}U). ^{6}He, ^{8}He and Li ions have been observed with average yields between $4 \cdot 10^{-5}$ and $2 \cdot 10^{-3}$ per antiproton annihilation. Proton evaporation from fission fragments after antiproton annihilation in ^{238}U is indicated by the low-energy cut-off of the proton spectrum.

We wish to thank K. Dietrich for valuable discussions, H. Hagn, D. Maier and H. Weiß for technical support, P. Stoeckel for graphical help, P. Maier-Komor for the preparation of some of the targets, the Karlsruhe group (PS 176) for the ^{40}Ca target, B. Dropesky for the ^{63}Cu target, T. Mayer-Kuckuk, H. Mommsen and the Institut für Strahlen- und Kernphysik of the University of Bonn for test measurements, A. Nilsson for collaboration, and the LEAR crew for very good experimental conditions. This work was supported by the Bundesministerium für Forschung and Technologie, Bonn, by the U.S. Department of Energy and by the U.S. National Science Foundation.

References

1) A.S. Iljinov, V.I. Nazaruk and S.E. Chigrinov, Nucl. Phys. **A382** (1982) 378
2) B. Povh and T. Walcher, Comments Nucl. Part. Phys. **16** (1986) 85
3) J. Rafelski, Phys. Lett. **B91** (1980) 281
4) D. Strottman, Phys. Lett. **B119** (1982) 39
5) M. Cahay, J. Cugnon, P. Jasselette and J. Vandermeulen, Phys. Lett. **B115** (1982) 7
6) M.R. Clover, R.M. DeVries, N.J. DiGiacomo and Y. Yariv, Phys. Rev. **C26** (1982) 2138
7) J. Cugnon and J. Vandermeulen, Phys. Lett. **B146** (1984) 16
8) D. Strottman and W.R. Gibbs, Phys. Lett. **B149** (1984) 288
9) P.L. McGaughey, M.R. Clover and N.J. DiGiacomo, Phys. Lett. **B166** (1986) 264
10) C. Baltay, P. Franzini, G. Lütjens, J.C. Severiens, D. Tycko and D. Zanello, Phys. Rev. **145** (1966) 1103
11) J.P. Bocquet, M. Epherre-Rey Campagnolle, G. Ericsson, T. Johansson, J. Konijn, T. Krogulski, M. Maurel, E. Monnand, J. Mougey, H. Nifenecker, P. Perrin, S. Polikanov, C. Ristori and G. Tibell, Phys. Lett. **B182** (1986) 146
12) E.F. Moser, H. Daniel, T. von Egidy, F.J. Hartmann, W. Kanert, G. Schmidt, M. Nicholas and J.J. Reidy, Phys. Lett. **B179** (1986) 25;
E.F. Moser, Thesis, Technische Universität München, Munich 1986 (unpublished)
13) J. Cugnon and J. Vandermeulen, Nucl. Phys. **A445** (1985) 717
14) J.F. Janni, At. Data Nucl. Data Tables **27** (1982) 341
15) H. Daniel, Nucl. Instr. Meth. **124** (1975) 253
16) J.F. Amann, P.D. Barnes, M. Doss, S.A. Dytman, R.A. Eisenstein, J. Penkrot and A.C. Thompson, Phys. Rev. Lett. **35** (1975) 1066
17) N.A. Burgov, M.K. Vlasov, L.S. Vorobev, S.A. Gerzon, Yu.T. Kiselev, M.V. Kosov, G.A. Leksin, A.N. Martemyanov, N.A. Pivnyuk, V.L. Stolin, Yu. V. Terekhov and V.I. Ushakov, Sov. J. Nucl. Phys. **24** (1976) 620
18) S.B. Kaufman, B.D. Wilkins, D.J. Henderson, R.E.L. Green, R.G. Korteling and G.W. Butler, Phys. Rev. **C32** (1985) 1977
19) H. Machner, Sa Jun, G. Riepe, D. Protic, H. Daniel, T. von Egidy, F.J. Hartmann, P. Hofmann, W. Kanert, W. Markiel, H. Plendl, K. Ziock, R. Marshall and J.J. Reidy, to be published
20) J.P. Bocquet, G. Ericsson, T. Johansson, J. Konijn, T. Krogulski, M. Maurel, E. Monnand, J. Mougey, H. Nifenecker, P. Perrin, S. Polikanov, M. Rey-Campagnolle, C. Ristori and G. Tibell, in "Physics at LEAR with low energy antiprotons", ed. C. Amsler *et al.* harwood academic publishers, Chur 1988, Nuclear Science Research Conference Series **14** (1988) 793
21) A. Angelopoulos, A. Apostolakis, T.A. Armstrong, B. Bassalleck, G. Bueche, M. Fero, M. Gee, N. Graf, H. Koch, R.A. Lewis, M. Mandelkern, P. Papaelias, H. Poth, H. Rozaki, L. Sakelliou, J. Schultz, J. Schwertel, G.A. Smith, T. Usher and D.M. Wolfe, Phys. Lett. **B205** (1988) 590
22) P. Jasselette, J. Cugnon and J. Vandermeulen, Nucl. Phys. **A484** (1988) 542
23) T. von Egidy, Nature **328** (1987) 773